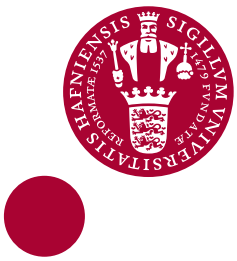

Knockin mouse with mutant G11 mimics human inherited hypocalcemia and is rescued by pharmacologic inhibitors

Roszko, Kelly L; Bi, Ruiye; Gorvin, Caroline M; Bräuner-Osborne, Hans; Xiong, Xiao-Feng; Inoue, Asuka; Thakker, Rajesh V; Strømgaard, Kristian; Gardella, Thomas; Mannstadt, Michael

Published in:
JCI insight

DOI:
10.1172/jci.insight.91079

Publication date:
2017

Document version
Publisher's PDF, also known as Version of record

JCI insight

RESEARCH ARTICLE

Knockin mouse with mutant $G\alpha_{11}$ mimics human inherited hypocalcemia and is rescued by pharmacologic inhibitors

Kelly L. Roszko,[1] Ruiye Bi,[1,2] Caroline M. Gorvin,[3] Hans Bräuner-Osborne,[4] Xiao-Feng Xiong,[4] Asuka Inoue,[5,6] Rajesh V. Thakker,[3] Kristian Strømgaard,[4] Thomas Gardella,[1] and Michael Mannstadt[1]

[1]Endocrine Unit, Massachusetts General Hospital and Harvard Medical School, Boston, Massachusetts, USA. [2]West China School of Stomatology, Sichuan University, Chengdu, Sichuan, China. [3]Academic Endocrine Unit, Radcliffe Department of Medicine, University of Oxford, Churchill Hospital, Oxford, England, United Kingdom. [4]Department of Drug Design and Pharmacology, University of Copenhagen, Copenhagen, Denmark. [5]Graduate School of Pharmaceutical Sciences, Tohoku University, Sendai, Japan. [6]Japan Science and Technology Agency (JST), Precursory Research for Embryonic Science and Technology (PRESTO), Kawaguchi, Saitama, Japan.

Heterotrimeric G proteins play critical roles in transducing extracellular signals generated by 7-transmembrane domain receptors. Somatic gain-of-function mutations in G protein α subunits are associated with a variety of diseases. Recently, we identified gain-of-function mutations in $G\alpha_{11}$ in patients with autosomal-dominant hypocalcemia type 2 (ADH2), an inherited disorder of hypocalcemia, low parathyroid hormone (PTH), and hyperphosphatemia. We have generated knockin mice harboring the point mutation *GNA11* c.C178T (p.Arg60Cys) identified in ADH2 patients. The mutant mice faithfully replicated human ADH2. They also exhibited low bone mineral density and increased skin pigmentation. Treatment with NPS 2143, a negative allosteric modulator of the calcium-sensing receptor (CASR), increased PTH and calcium concentrations in WT and mutant mice, suggesting that the gain-of-function effect of $GNA11^{R60C}$ is partly dependent on coupling to the CASR. Treatment with the $G\alpha_{11/q}$-specific inhibitor YM-254890 increased blood calcium in heterozygous but not in homozygous $GNA11^{R60C}$ mice, consistent with published crystal structure data showing that Arg60 forms a critical contact with YM-254890. This animal model of ADH2 provides insights into molecular mechanism of this G protein–related disease and potential paths toward new lines of therapy.

Introduction

Heterotrimeric G proteins are critical signal transducers of activated G protein coupled receptors (GPCRs) (1). Gain-of-function mutations in several different Gα subunits — $G\alpha_s$, $G\alpha_i$, $G\alpha_{12/13}$, and $G\alpha_{11/q}$ — are associated with a wide range of human diseases. Two common sites of mutation are G.hfs2.2 in switch 1 and G.s3h2.3 in switch 2 (Arg201 and Gln227 in $G\alpha_s$, respectively) (2); such mutations are highly activating in vitro and often oncogenic in vivo (2, 3). Activating point mutations at either of these residues in $G\alpha_s$ cause a variety of clinical manifestations, including pituitary, thyroid, and adrenal tumors, as well as McCune-Albright syndrome (3). Activating mutations at the corresponding residues (Arg183 and Gln209) in either $G\alpha_{11}$ or $G\alpha_q$, are associated with ocular melanomas and congenital hemangioma, and those of $G\alpha_q$ are associated with Sturge-Weber syndrome (4–7). These highly activating Gα mutations occur somatically and are presumably lethal in the germline (8). The only reported germline activating mutation in $G\alpha_s$ is Ala366Ser (G.s6h5.3), reported in 2 patients with testotoxicosis; in this case, the mutant allele is temperature sensitive and, thus, only stable and active at the lower temperature of the testes (9).

Recently, we and others identified germline gain-of-function mutations in $G\alpha_{11}$, encoded by the *GNA11* gene, in families with autosomal-dominant hypocalcemia type 2 (ADH2) (10–14). To date, 6 such mutations have been uncovered in ADH2 patients (10–14). These mutations show weak effects in vitro when compared with the highly activating mutations discussed above (12). The principal phenotype in

Authorship note: KLR and RB contributed equally to this work.

Conflict of interest: MM is associated with Shire Pharmaceuticals (unrelated to this work). RT is associated with Shire/NPS Pharmaceuticals Inc. (USA), GlaxoSmithKline, Novartis Pharma AG, and Marshall-Smith Syndrome Foundation. KS is associated with Avilex Pharma (unrelated to this work).

Submitted: October 10, 2016
Accepted: January 3, 2017
Published: February 9, 2017

Reference information:
JCI Insight. 2017;2(3):e91079. https://doi.org/10.1172/jci.insight.91079.

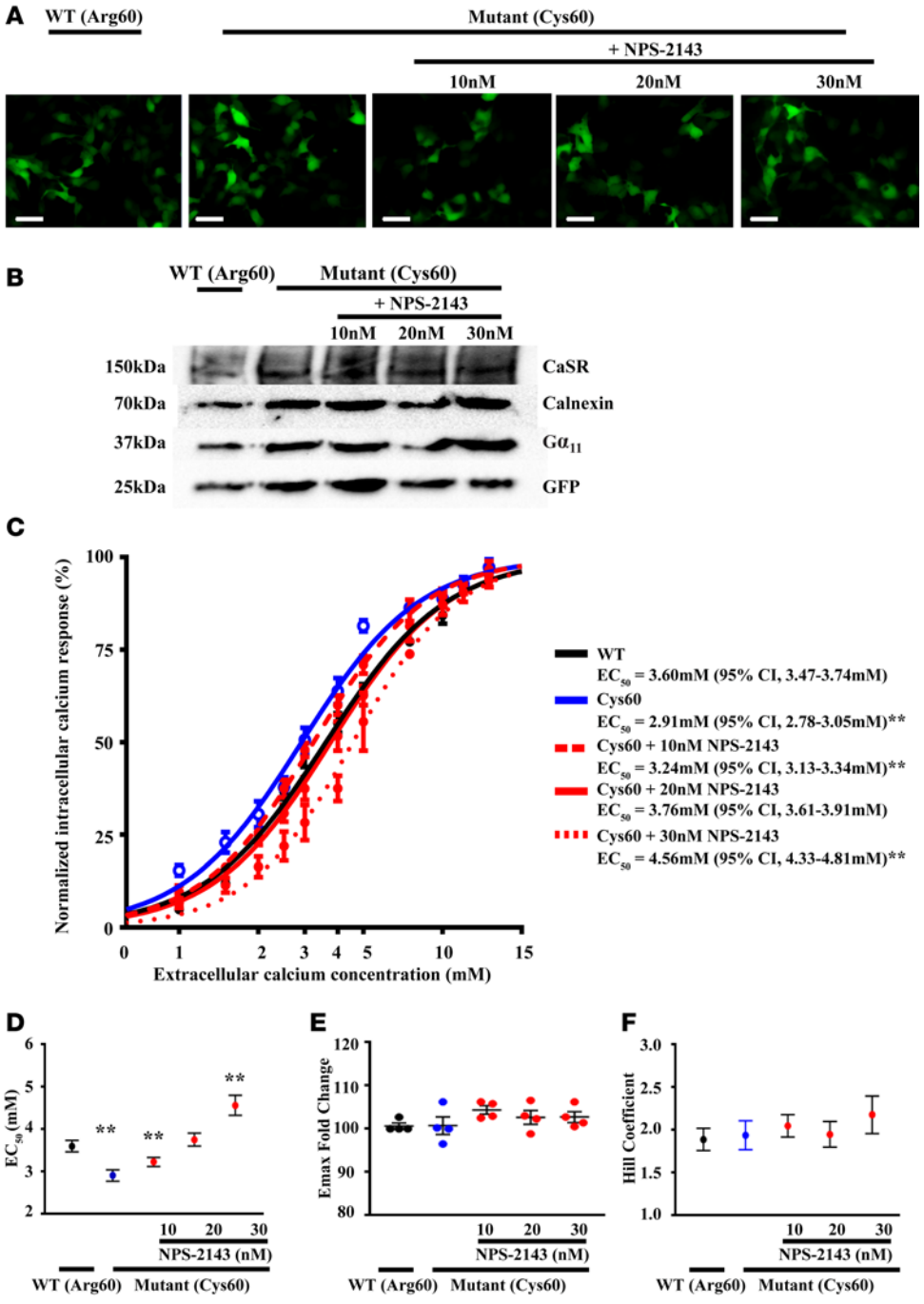

Figure 1. GNA11^{R60C} mutant increases Ca^{2+}_i responses, which can be normalized by the calcilytic NPS 2143. (**A**) Immunofluorescent images of HEK-CASR cells transiently transfected with WT (Arg60) or mutant (Cys60) pBI-CMV2-*GNA11* constructs. All constructs had similar expression of GFP. Scale bars: 10μm. (**B**) Western blot analysis of lysates from HEK-CASR cells used for flow cytometry experiments. All cells expressed $G\alpha_{11}$ and GFP at similar levels. Calnexin was used as a housekeeping protein. (**C**) Concentration-response curves showing normalized Ca^{2+}_i responses to increasing doses of $[Ca^{2+}]_o$ in HEK-CASR cells expressing WT or GNA11^{R60C} constructs. Mutant (Cys60) had a leftward shift in the concentration-response curve (blue, solid line, open circles) when compared with WT (Arg60; black, solid line, closed circles). Treatment of GNA11^{R60C} expressing cells with increasing doses of the negative allosteric modulator NPS 2143 (red, dotted lines) led to a rightward shift in the dose response curves toward WT (Arg60) levels. (**D**) The GNA11^{R60C} mutant (blue bar) was associated with reduced EC_{50} values compared with WT $G\alpha_{11}$ (black bar). Treatment of GNA11^{R60C}-expressing cells led to an increase in EC_{50} values, which was normalized to WT (Arg60) levels with a 20 nM dose. (**E**) The GNA11^{R60C} mutant (blue bar) and NPS 2143–treated cells had similar maximal responses (Emax) to WT (Arg60) cells. (**F**) The GNA11^{R60C} mutant (blue bar) and NPS 2143–treated cells had similar Hill coefficient values to WT (Arg60) cells. Data is expressed as mean ± SEM. $^{**}P < 0.02$. Experiments were performed in 4 independent transfections.

the patients with these $G\alpha_{11}$ mutations is a perturbation in calcium homeostasis. The clinical findings of ADH2 implicate the involvement of the calcium-sensing receptor (CASR), which can couple to several G proteins, including $G\alpha_{11}$, and is expressed on the surface of the parathyroid chief cells. Activation of the CASR suppresses production and secretion of parathyroid hormone (PTH), a principal calcium-regulating hormone that increases blood calcium through effects on bone and kidney (15, 16). Activating mutations in *CASR* cause ADH1, in which hypocalcemia is observed with inappropriately low circulating PTH levels, resembling the clinical phenotype of ADH2 (17). The CASR is also expressed in the renal distal tubule, where it acts independently of PTH to promote calcium excretion (18). Consequently, a further complication of ADH1 is hypercalciuria, which results from the combined effects of reduced PTH signaling and increased CASR signaling in the renal distal tubule cells (19).

The *GNA11* gene is almost ubiquitously expressed; therefore, it is remarkable that the main clinical manifestation associated with germline gain-of-function mutations in *GNA11* is an abnormality in calcium regulation. Studies in transfected cells show that the gain-of-function $G\alpha_{11}$ mutations of ADH2

Figure 2. Mutant mice with activating $G\alpha_{11}$ have darker ear and tail color. (**A** and **B**) Increased tail and ear pigmentation of the mutant mice compared with WT littermates at age 12–13 weeks. Homozygous GNA11$^{R60C/R60C}$ mice had darker color of their tails and ears than heterozygous GNA11$^{R60C/WT}$ mice.

each result in a small but significant increase in the sensitivity with which the CASR responds to extracellular calcium, an effect that likely accounts for the perturbations in PTH secretion and calcium homeostasis seen in patients (11–13). Short stature has been reported in affected individuals from two families (12, 14), suggesting possible effects on growth. The number of reported patients with ADH2 is limited, however, such that additional disease phenotypes may exist. Furthermore, the best treatment options for patients with *GNA11* mutations are still unclear. We therefore generated a knockin mouse model of ADH2 with a germline *GNA11* c.C178T point mutation (p.Arg60Cys), which was identified in a family affected with ADH2 (10). We report here the phenotypic properties of the mutant mice, as well as their response to treatment with two inhibitors with relevance to the disease; the small molecule calcilytic drug, NPS 2143, which acts as a negative allosteric modulator (NAM) of the CASR and thereby can induce increased PTH secretion (20, 21); and the cyclic depsipeptide YM-254890, which acts as a competitive inhibitor of $G\alpha_{11/q}$ (22–24).

Results

Effect of the GNA11^{R60C} mutation on Ca^{2+}_i responses in vitro. To determine the effects of the Arg60Cys mutation on CASR-mediated signaling, WT HEK293 cells stably expressing the CASR (HEK-CASR) were transiently transfected with a pBI-CMV2 plasmid that encoded either the WT (Arg60) or mutant (Cys60) $G\alpha_{11}$ protein. Expression levels of the CASR, $G\alpha_{11}$, and GFP proteins were assessed by fluorescence microscopy and/or Western blot analyses (Figure 1, A and B). Calnexin was used as a loading control in Western blot analyses, which showed similar expression levels for WT and mutant $G\alpha_{11}$ proteins, both in the presence and absence of NPS 2143 (Figure 1B). To assess function of the WT and mutant $G\alpha_{11}$ proteins, we measured changes in intracellular calcium (Ca^{2+}_i) in response to alterations in extracellular calcium ($[Ca^{2+}]_o$) by flow cytometry (11, 13). The Ca^{2+}_i responses in WT and mutant $G\alpha_{11}$-expressing cells were shown to increase in a dose-dependent manner following stimulation with increasing concentrations of Ca^{2+}_o, and the responses in the mutant GNA11^{R6OC}-expressing cells were significantly left-shifted as compared with those in the GNA11^{WT}-expressing cells (Figure 1, C and D; EC_{50} = 2.91 mM [95% CI, 2.78–3.05 mM] for Arg60, compared with 3.60 mM [95% CI, 3.47–3.74 mM] for WT; $P < 0.02$), whereas the maximal signaling responses and Hill coefficients of WT and Cys60 mutant–expressing cells were similar (Figure 1, E and F). These findings confirm that the GNA11^{R6OC} mutant exerts a gain-of-function effect on CASR signaling and, thus, enhances the receptor's sensitivity to Ca^{2+}_o (11–13).

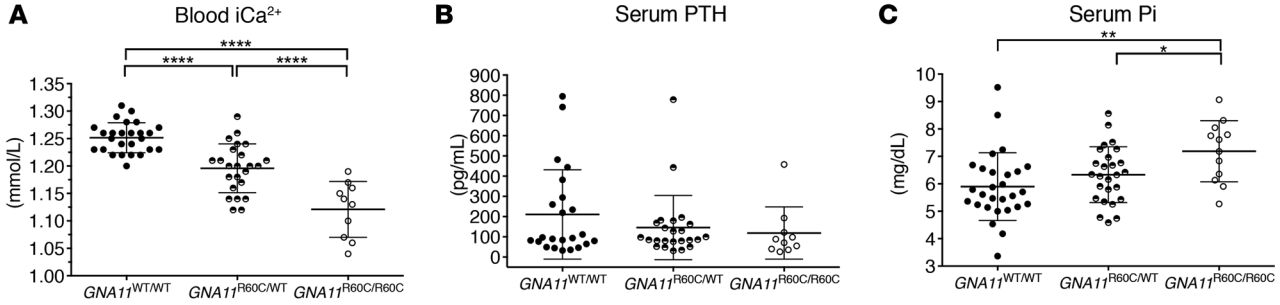

Figure 3. Knockin mice with activated $G\alpha_{11}$ (*GNA11*^{R60C} mutation) were hypocalcemic and hyperphosphatemic with inappropriately low parathyroid hormone (PTH) levels. Biochemical parameters of 9-week-old *GNA11*$^{WT/WT}$ mice (n = 26–28), *GNA11*$^{R60C/WT}$ heterozygous mice (n = 24), and *GNA11*$^{R60C/R60C}$ homozygous mice (n = 10). (**A**) Ionized calcium (iCa^{2+}), (**B**) serum PTH, (**C**) serum phosphate (Pi) (*$P < 0.05$, **$P < 0.01$, ****$P < 0.0001$, using a one-way ANOVA test with Tukey's multiple corrections). Data is reported as mean ± SD.

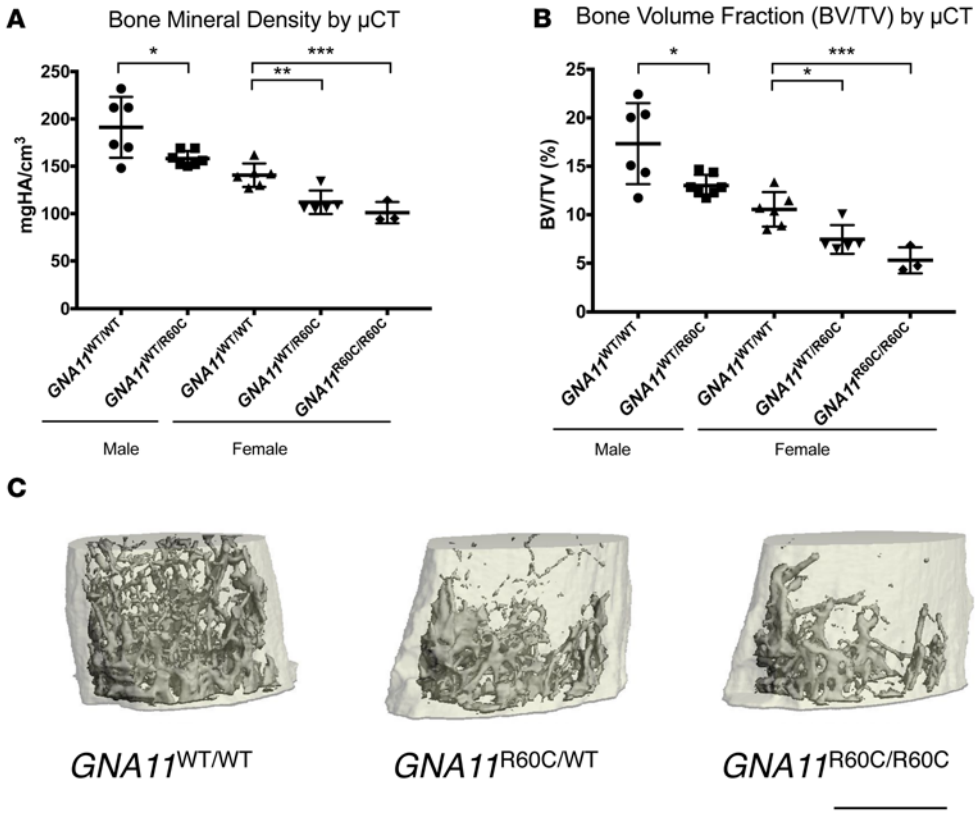

Figure 4. Mutant mice have reduced bone mineral density and bone volume fraction. μCT analysis revealed significant decreases in bone mineral density (BMD) (**A**) and bone volume fraction (BV/TV) (**B**) in 12- to 13-week-old male *GNA11*$^{R60C/WT}$ (n = 7) vs. *GNA11*$^{WT/WT}$ (n = 6); female *GNA11*$^{R60C/WT}$ (n = 5) vs. *GNA11*$^{WT/WT}$ (n = 6), and female *GNA11*$^{R60C/R60C}$ (n = 3) vs. *GNA11*$^{WT/WT}$ (n = 6) mice. Data are shown as mean ± SD. Only 1 male *GNA11*$^{R60C/R60C}$ survived to μCT analysis. This mouse showed a BMD of 185 mgHA/cm^3 and BV/TV of 16.33% (Supplemental Figure 1). The 3 groups of female mice were analyzed by ANOVA with Tukey's multiple comparisons tests, and the 2 groups of male mice were analyzed by Student's t test. (*P < 0.05, **P < 0.01, ***P < 0.005). (**C**) μCT image of the distal femur of representative 12-week-old female mice. Scale bar: 1 mm.

Effect of the calcilytic NPS 2143 on the gain-of-function associated with the GNA11^{R6OC} mutation in vitro. To investigate whether allosteric inhibition of the CASR might rectify the gain-of-function effect imposed by the GNA11^{R6OC} mutation, the effect of the NPS 2143 calcilytic compound on CASR signaling was examined in HEK-CASR cells expressing either WT Gα_{11} or mutant (Cys60) Gα_{11} proteins. NPS 2143 was used at 10, 20, and 30 nM concentrations, as similar doses of this calcilytic have been reported to rectify the altered signaling responses associated with different ADH2-causing Gα_{11} mutations (25) as assessed in similar cell-based assays (21). Consistent with these previous studies, NPS 2143 increased the EC_{50} of Gα_{11}-Cys60–expressing mutant cells in a dose-dependent manner. Thus, 20 nM of NPS 2143 increased the EC_{50} of Cys60-expressing mutant cells from 2.91 mM (95% CI, 2.78–3.05 mM) in untreated cells to 3.76 mM (95% CI, 3.61–3.91 mM), which was not significantly different from the EC_{50} of 3.60 mM (95% CI, 3.47–3.74 mM) for WT cells; and 30 nM of NPS 2143 increased the EC_{50} of the mutant cells to 4.56 mM (95% CI, 4.33–4.81 mM), which was significantly greater than that of WT cells (Figure 1, C and D). NPS 2143 had no effect on the maximal signaling responses or Hill coefficients of WT or mutant Gα_{11}-expressing cells. Thus, the findings of these in vitro studies demonstrate that NPS 2143 can rectify the gain-of-function effect associated with the GNA11^{R6OC} mutation.

Phenotype of GNA11^{R60C} mice. Through CRISPR-Cas9 methodology, we successfully generated knockin mice with the GNA11^{R6OC} mutation. Founder mice (8%) harbored the correct *GNA11* c.C178T mutation generated by homology-directed repair. We confirmed by direct sequencing of PCR products that F1 generation mice carried one *GNA11*^{R60C} allele and one WT allele (data not shown). Three independent mouse lines gave indistinguishable results (data not shown). Intercrossing *GNA11*^{R60C} heterozygous F1 mice yielded a slightly lower number of heterozygous and homozygous mice as compared with WT mice at the time of weaning than would be expected by Mendelian genetics (Table 1).

Increased pigmentation of tails and ears was noted in *GNA11*^{R60C} mutant adult mice with an apparent gene-dosage effect (Figure 2). Body length and weight were similar between 13-week-old mutant mice and their same-sex WT littermates.

Homozygous and heterozygous mice had significantly lower serum ionized calcium (iCa^{2+}) compared with age-matched WT animals (1.12 ± 0.05 mmol/l vs. 1.20 ± 0.04 mmol/l vs. 1.25 ± 0.03 mmol/l; mean ± SD; P < 0.0001; Figure 3). PTH levels (mean ± SD) were similar in both the heterozygous (146 ± 159 pg/ml) and homozygous mice (119 ± 129 pg/ml) as compared with WT mice (211 ± 221 pg/ml) and therefore

Table 1. Observed vs. expected number (percentage) of *GNA11*$^{WT/WT}$, *GNA11*$^{R60C/WT}$ heterozygous, and *GNA11*$^{R60C/R60C}$ homozygous animals from heterozygous matings at the time of weaning.

GNA11$^{R60C/WT}$ × *GNA11*$^{R60C/WT}$	WT	*GNA11*$^{R60C/WT}$	*GNA11*$^{R60C/R60C}$
Expected Mice	15 (25%)	30 (50%)	15 (25%)
Viable Mice	24 (40%)	26 (43%)	10 (17%)

The observed distribution differed from the expected (25% WT, 50% heterozygous, 25% homozygous) (χ^2 statistic 7.6, 2 degrees of freedom, $P = 0.022$).

inappropriate, given the degree of hypocalcemia. As frequently found in hypoparathyroid patients, serum phosphate was significantly higher in the homozygous *GNA11*$^{R60C/R60C}$ mice (7.19 ± 1.11 mg/dl) as compared with either WT (5.90 ± 1.24 mg/dl) or heterozygous *GNA11*$^{R60C/WT}$ mice (6.33 ± 1.02 mg/dl) (mean ± SD).

μCT analysis revealed significantly lower bone mineral density (BMD) and bone volume/total volume (BV/TV) in both female (heterozygous and homozygous) and male (heterozygous) mice compared with WT mice at age 12–13 weeks (Figure 4 and Table 2). Only 1 male GNA11$^{R60C/R60C}$ mouse was available for μCT analysis at age 12–13 weeks, but at age 20 weeks, male homozygous mice had a significantly lower BMD and BV/TV as compared with WT mice (Supplemental Figure 1; supplemental material available online with this article; http://doi.org/10.1172/jci.insight.91079DS1). In 12- to 13-week-old female mutant mice, the trabecular number (Tb.N) was decreased and trabecular spacing (Tb.Sp) increased in a gene dosage–dependent pattern. Compared with WT mice, cortical thickness (Ct.Th) was also significantly decreased in the female mutant mice (Table 2). Whole-body and hind limb BMD of 12-week-old mice measured by dual-energy X-ray absorptiometry (DXA) was significantly lower in female heterozygous and homozygous compared with WT mice (Supplemental Figure 2), but in male mice, differences did not reach significance (Supplemental Figure 2).

There was no significant difference in fasting spot urinary fractional excretion index of calcium (FEICa) (Figure 5) or urinary calcium/creatinine ratio (Supplemental Figure 3) between any of the groups.

Treatment of mice with the calcilytic NPS 2143. Four hours after i.p. injection of NPS 2143, serum ionized calcium and PTH concentration significantly increased in WT, *GNA11*$^{R60C/WT}$, and *GNA11*$^{R60C/R60C}$ mice compared with their respective baseline levels and compared with vehicle-treated controls (Figure 6 and Supplemental Table 1). Twenty-four hours after the injection, the ionized calcium level of the WT mice treated with the calcilytic was still elevated compared with vehicle ($P = 0.02$), but there was no longer a difference between the calcilytic and vehicle groups in the mutant animals. Serum phosphate levels increased significantly in WT mice 4 hours after treatment with NPS 2143 but not in the NPS 2143–treated *GNA11*$^{R60C/WT}$ or *GNA11*$^{R60C/R60C}$ mice. The fasting spot urinary FEICa was significantly decreased in the *GNA11*$^{R60C/WT}$ and *GNA11*$^{R60C/R60C}$ mice at 4 hours after treatment with the calcilytic (Figure 5). There was no change in the urinary calcium/creatinine ratio between any of the groups (Supplemental Figure 3).

Treatment of mice with the $G\alpha_{11/q}$ inhibitor YM-254890. Four hours after single-dose i.p. injection of YM-254890, there was a significant increase in the serum ionized calcium concentration in the WT mice (Figure 7, A–C, and Supplemental Table 2). Heterozygous *GNA11*$^{R60C/WT}$ mice treated with YM-254890 also had an increase in cal-

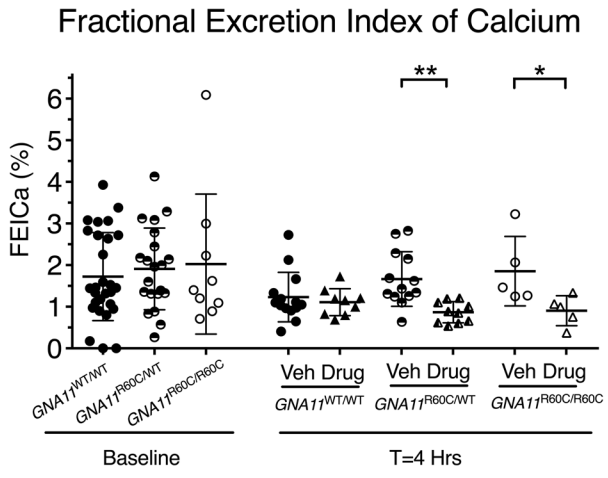

Figure 5. Decrease in the fractional excretion index of calcium after treatment of mice with a single injection of a calcilytic. Fractional excretion of calcium was determined in WT (*GNA11*$^{WT/WT}$, $n = 28$ baseline, $n = 14$ vehicle, $n = 9$ calcilytic), heterozygous (*GNA11*$^{R60C/WT}$, $n = 21$ baseline, $n = 13$ vehicle, $n = 10$ calcilytic), or homozygous mice (*GNA11*$^{R60C/R60C}$, $n = 9$ baseline, $n = 5$ vehicle, $n = 5$ calcilytic) at baseline and 4 hours after bolus i.p. injection of either vehicle (Veh) or 28 mg/kg of the calcilytic NPS 2143 (Drug). Data are shown as mean ± SD. At baseline, results for the 3 genotypes were analyzed using one-way ANOVA with Tukey's multiple corrections. At 4 hours, vehicle- and calcilytic-treated groups were compared by Student's *t* test. (*$P < 0.05$, **$P < 0.01$).

Table 2. Bone mineral density (BMD) and trabecular and cortical microarchitecture at 12–13 weeks of age in WT *GNA11*$^{WT/WT}$, heterozygous *GNA11*$^{R60C/WT}$, or homozygous *GNA11*$^{R60C/R60C}$ mutant mice.

	BMD (mgHA/cm^3)	BV/TV (%)	Tb.N (1/mm)	Tb. Th (mm)	Ct.Th (mm)	Ct.Ar (mm^2)	Tt.Ar (mm^2)
Female WT (n = 6)	140 ± 12^{AB}	10.55 ± 1.78^{AB}	3.587 ± 0.305^{AB}	0.051 ± 0.003	0.150 ± 0.009^{AB}	0.628 ± 0.041^{B}	1.624 ± 0.067
GNA11$^{R60C/WT}$ (n = 5)	112 ± 12^{A}	7.45 ± 1.47^{A}	2.815 ± 0.596^{AC}	0.050 ± 0.003	0.136 ± 0.006^{A}	0.567 ± 0.052	1.569 ± 0.146
GNA11$^{R60C/R60C}$ (n = 3)	101 ± 11^{B}	5.31 ± 1.33^{B}	1.879 ± 0.402^{BC}	0.051 ± 0.003	0.131 ± 0.004^{B}	0.533 ± 0.031^{B}	1.503 ± 0.136
Male WT (n = 6)	191 ± 32^{A}	17.34 ± 4.19^{A}	4.821 ± 0.353	0.056 ± 0.010	0.151 ± 0.008	0.675 ± 0.055	1.765 ± 0.078
GNA11$^{R60C/WT}$ (n = 7)	159 ± 8^{A}	13.12 ± 1.16^{A}	4.504 ± 0.290	0.049 ± 0.003	0.147 ± 0.009	0.643 ± 0.029	1.705 ± 0.052
GNA11$^{R60C/R60C}$ (n = 1)	185	16.33	4.78	0.05	0.152	0.598	1.460

Bone parameters as reported from μCT analysis of WT, heterozygous, and homozygous *GNA11*$^{R60C/R60C}$ mice. All statistics were by ANOVA with Tukey's multiple comparisons tests. ($^{A}P < 0.05$ WT vs. heterozygous; $^{B}P < 0.05$ WT vs. homozygous; $^{C}P < 0.05$ heterozygous vs. homozygous). BV/TV, bone volume/total volume; Tb.N, trabecular network; Tb.Th, trabecular thickness; Ct.Th, cortical thickness; Ct.Ar, cortical area; Tt.Ar, total cross-sectional area.

cium as compared with vehicle-treated mice, but the effect did not quite reach statistical significance (P = 0.06). The homozygous *GNA11*$^{R60C/R60C}$ mice exhibited no change in blood ionized calcium concentration in response to YM-254890 treatment. Mean PTH levels increased significantly in the WT mice after injection of YM-254890, but individual levels varied and some mice had no increase in PTH. YM-254890 induced no significant change in PTH levels in the heterozygous or homozygous mice (Figure 7, D–F). Levels of serum phosphate and urinary fractional excretion of calcium were unchanged in any of the groups at 4 hours after treatment with YM-254890 as compared with treatment with vehicle (Figure 7, G–I, and Supplemental Table 2).

Inhibition of iCa^{2+} signaling through $G\alpha_{11/q}$ in vitro using YM-254890. Consistent with the lack of efficacy of the $G\alpha_{11/q}$ inhibitor in mice homozygous for GNA11^{R6OC}, in vitro studies showed that YM-254890 had no effect on Ca^{2+}_i signaling mediated by another GPCR, the PTH1R, in HEK-293–derived cells expressing GNA11^{R6OC} (Figure 8). The PTH1R was used for this in vitro analysis, as we found it to give more robust agonist-induced Ca^{2+}_i responses than the CASR or the endogenous P2Y1 purinergic receptors stimulated with $[Ca^{2+}]_o$ and ADP, respectively, and thus could better reveal effects of the inhibitor compound (data not shown). When GNA11^{WT} was introduced into HEK cells lacking functional $G\alpha_{11/q}$, PTH-induced stimulation of Ca^{2+}_i signaling via the PTH1-receptor in HEK cells was fully inhibited by YM-254890.

Discussion

This study reports the generation, through CRISPR-Cas9 technology, of a mouse model of ADH2 harboring a knockin of the activating mutation GNA11^{R6OC}, discovered in a family with the disease (10). These mice faithfully replicate ADH2 and enable a more in-depth analysis of the effects of the GNA11^{R6OC} mutation on tissue-specific phenotypes, as well as the potential for selected inhibitor compounds to modify or correct the ADH2 phenotype. Our in vitro studies with HEK cells stably expressing the CASR confirmed that GNA11^{R6OC} exerts a gain-of-function effect on CASR signaling, in that the mutant protein caused a leftward shift in the calcium dose–response curve, indicating an increased sensitivity to $[Ca^{2+}]_o$. This gain-of-function effect of the $G\alpha_{11}$ mutant on CASR signaling is consistent with the effects observed for other $G\alpha_{11}$ mutations identified in ADH2 and, mechanistically, can explain the hypocalcemic and hyperphosphatemic disturbances seen in ADH2 patients (10–14), which are fully recapitulated in the *GNA11*^{R60C} mutant mice. The results, thus, establish that the mutation is sufficient to cause ADH2 and provide a plausible mechanistic basis of the disease.

ADH2 in humans follows a heterozygous, autosomal-dominant mode of inheritance. Compared with heterozygous mice, homozygous ADH2 mice showed more severe abnormalities in all parameters measured. Thus, there was a clear gene-dosage effect of the Arg60Cys mutation on the calcium, phosphate, and bone homeostasis. In 3 independent breeding lines, we observed a lower-than-expected proportion of viable animals with the ADH2 mutation. This suggests a possible survival disadvantage conferred by the mutation. In humans, highly activating gain-of-function Gα mutations are only encountered as somatic mutations, often in tumors, and are not transmitted through the germline. Interestingly, a transgenic mouse with a heritable $G\alpha_s^{R201C}$ mutation has been described (26). Compared with such oncogenic mutations, which affect residues Arg183 and Gln209 ($G\alpha_{11/q}$ nomenclature) that are directly involved in GTP catalysis,

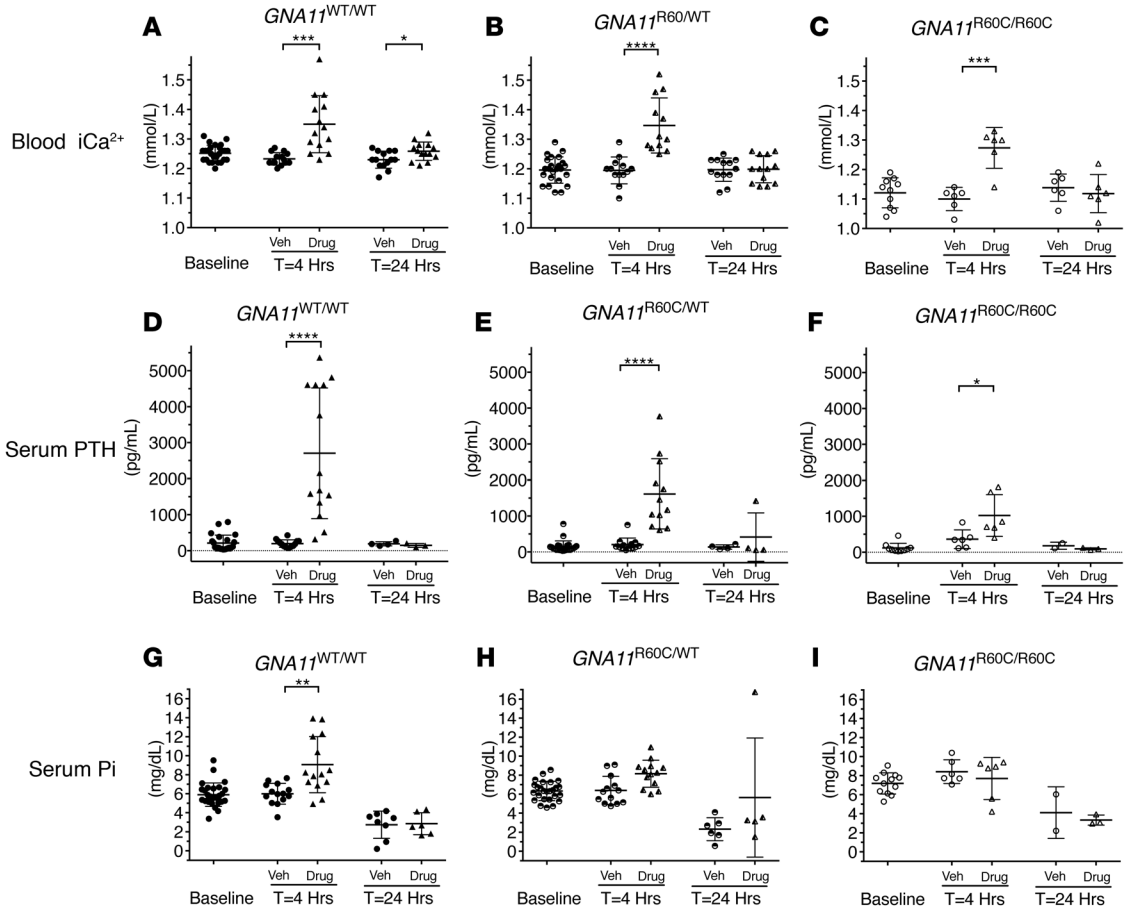

Figure 6. Calcium and parathyroid hormone (PTH) increased significantly after injection of the calcilytic in WT mice and mice with activating $G\alpha_{11}$. (**A–C**) Biochemical parameters at baseline and 4 and 24 hours after bolus i.p. injection of the calcilytic NPS 2143 (Drug) at 28 mg/kg or vehicle (Veh) in 9-week-old *GNA11*$^{WT/WT}$ (n = 14 vehicle, n = 14 calcilytic), *GNA11*$^{R60C/WT}$ (n = 13 vehicle, n = 13 calcilytic), and *GNA11*$^{R60C/R60C}$ (n = 6 vehicle, n = 6 calcilytic) mice. (**A–C**) blood iCa^{2+}, (**D–F**) serum PTH, (**G–I**) serum Pi. Data are shown as mean ± SD. (*P < 0.05, **P < 0.01, ***P < 0.001, ****P < 0.0001, using Student's t test).

the gain-of-function $G\alpha_{11}$ mutations of ADH2 — which affect residues more distant from the GTPase site (Figure 8D) — appear to have milder effects on G protein function (12); this may explain why these mutations are sufficiently tolerated to allow germline transmission.

Hypercalciuria and the attendant risk of nephrocalcinosis are potential complications for patients with ADH1, in which the combined effects of enhanced CASR signaling in the parathyroid glands and in the renal distal tubules can result in marked increases in calcium excretion (19, 27). In principle, ADH2 patients would also be expected to exhibit elevated levels of calcium excretion, but data are limited and variable (10–14). In our estimates of urinary fractional excretion of calcium, we detected no difference between WT and the hypocalcemic heterozygous and homozygous mutant ADH2 mice at baseline while fasting. There was also no difference in the spot urine calcium/creatinine ratio between the groups of animals. While the lack of difference in fractional excretion of calcium at baseline in a steady state could indicate that the activated $G\alpha_{11}$ mutant does not have a dominant effect on CASR function in the renal distal tubule cells, more extensive analyses — for example, involving 24-hour urine collections — are needed to resolve such potential effects of the mutation on renal function. In any case, it is clear that the mutant $G\alpha_{11}$ impacted CASR signaling in the parathyroid glands, as the ADH2 mice were significantly hypocalcemic with reduced or inappropriately normal serum PTH levels.

The hypocalcemic phenotype of patients and animals with ADH2 is best explained by the effects of gain-of-function $G\alpha_{11}$mutations on signaling through the CASR receptor. In this model, the mutant $G\alpha_{11}$ leads to increased intracellular signaling when the CASR is activated by $[Ca^{2+}]_o$. The effects of the mutant $G\alpha_{11}$ would, thus, overlap with those caused by activating mutations in the CASR. Given that $G\alpha_{11}$ can likely

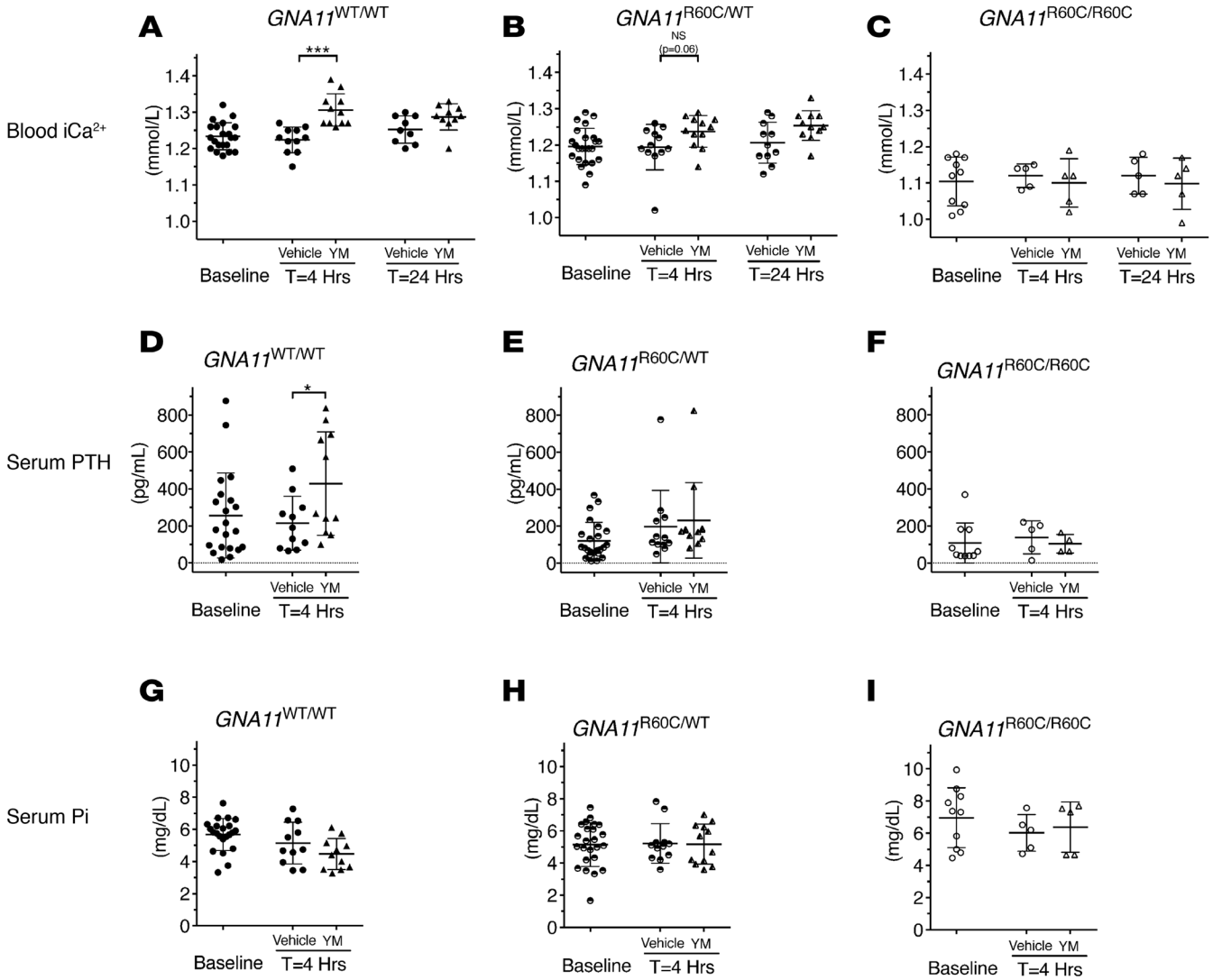

Figure 7. Treatment of mice with single bolus injection of $G\alpha_{11/q}$ inhibitor (YM-254890). iCa^{2+} and parathyroid hormone (PTH) increased in WT and heterozygous *GNA11*$^{R60C/WT}$ but not homozygous *GNA11*$^{R60C/R60C}$ mice. Biochemical parameters at baseline and 4 hours after bolus i.p. injection of YM-254890 at 0.15 mg/kg or vehicle in 12-week-old *GNA11*$^{WT/WT}$ (n = 11 vehicle, n = 11 YM-254890), *GNA11*$^{R60C/WT}$ (n = 12 vehicle, n = 12 YM-254890), and *GNA11*$^{R60C/R60C}$ (n = 5 vehicle, n = 5 YM-254890) mice. (**A–C**) blood iCa^{2+}, (**D–F**) serum PTH, (**G–I**) serum Pi. Data are shown as mean ± SD (*P < 0.05, ***P < 0.001, using Student's t test).

couple to a number of other GPCRs, it seems rather surprising that ADH2 patients do not show broader effects of the mutation beyond calcium homeostasis. We did, however, observe several additional phenotypic traits in the ADH2 mutant mice, including darker skin coloration readily visible on the tail and ears. This trait closely matches that seen in the "dark skin" mouse strain, Dsk7, which also harbors a moderately activating mutation (Ile62Val, previously listed as Ile63Val) in $G\alpha_{11}$; in this case, the endothelin receptor B (ENDR-B) was suggested as a key codeterminant of the increased skin pigmentation (28). While no patient with a $G\alpha_{11}$ gain-of-function mutation has yet been reported to have increased skin pigmentation, our data suggest that, in mice, the human GNA11^{R6OC} mutant of ADH2 can alter at least some GPCR signaling pathways other than the CASR, including those probably involving ENDR-B.

The decreased BMD in the mutant ADH2 mice is also of interest. This finding is notably different from the increased BMD typically present in patients with other forms of hypoparathyroidism (29, 30). It is also different from the findings of increased BMD in knockin mice expressing an activated CASR mutant (31). By contrast, transgenic mice expressing an oncogenic variant of the closely related $G\alpha_q$ ($G\alpha_q^{Q207L}$) in osteoblasts through the *col. 1* promoter have osteoporosis (32), and related studies in vitro show that activation of $G\alpha_q$ signaling inhibits osteoblast differentiation (32). Thus, it is plausible that the GNA11^{R6OC} mutant

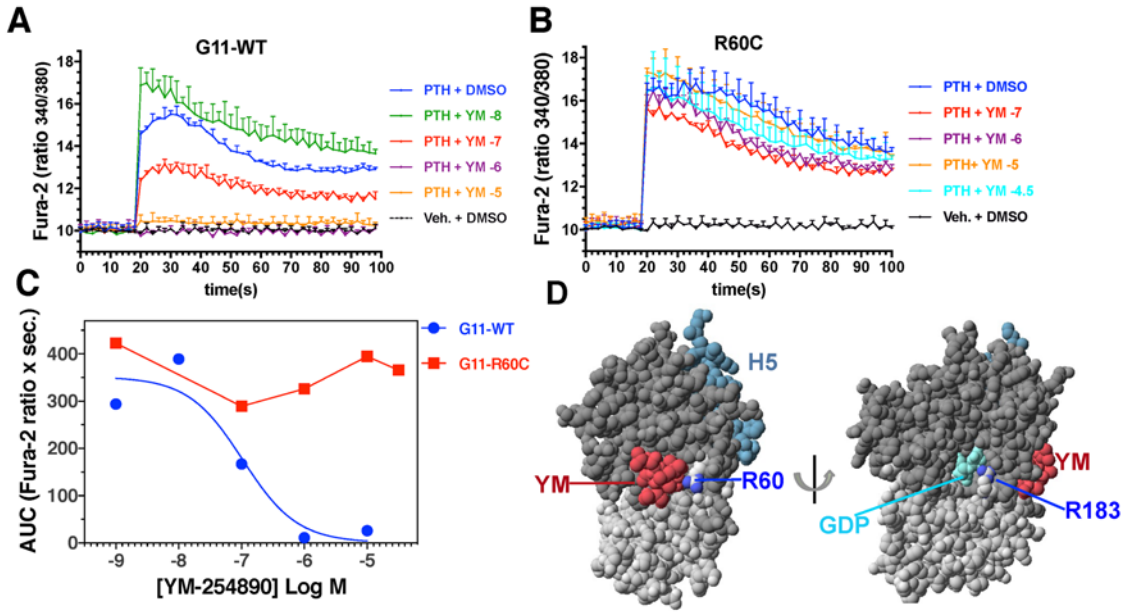

Figure 8. YM-254890 fully inhibited parathyroid hormone–induced (PTH-induced) stimulation of Ca^{2+}_i signaling via the PTH1 receptor in HEK cells transfected with GNA11^{WT} but not with GNA11^{R60C}. Fura-2–treated HEK-293–derived cells in which the genes encoding the endogenous $G\alpha_q$ and $G\alpha_{11}$ were knocked out were cotransfected with plasmids encoding either $G\alpha_{11}^{R60C}$ (**A**) or $G\alpha_{11}^{WT}$ (**B**), along with the PTHR1. Forty-eight hours after transfection, cells were pretreated for 45 minutes with Fura-2,AM at a concentration of 5×10^{-6} M, together with either DMSO (0.1%) or DMSO containing YM-254890 at the indicated concentration and then treated with vehicle (Veh.) or PTH(1-34) (1×10^{-7} M) and analyzed for changes in Ca^{2+}_i signaling: blue line, PTH + DMSO; green line, PTH + 1×10^{-8} M YM-254890; red line, PTH + 1×10^{-7} M YM-254890; purple line, PTH + 1×10^{-6} M YM-254890; orange line, PTH + 1×10^{-5} M YM-254890; aqua line, PTH + $1 \times 10^{-4.5}$ M YM-254890; black line, Vehicle + DMSO. Ratiometric Fura-2 fluorescence was measured using an Envision plate reader. Data are means (± SEM) of duplicate wells from a single experiment; 2 other replicate experiments yielded comparable results. (**C**) Dose-response curves for YM-254890 generated by plotting the AUC for each PTH-induced response observed in the absence or presence of inhibitor in the experiments of panels **A** and **B**. (**D**) Model of $G\alpha_q$ in complex with YM-254890. The orientation on the left shows the close proximity of Arg60, mutated in ADH2, with YM-254890 (red), and the orientation on the right shows the close proximity of Arg183, at which more strongly activating oncogenic mutations occur, with bound guanine nucleotide GDP (cyan). The side chain nitrogens of Arg60 and Arg180 are colored blue; the RAS and helical portions of the G protein are shaded dark and light gray, respectively, and helix-5 of the RAS domain, which participates in GPCR interaction, is shaded aqua. The model was prepared using the x-ray coordinate file PDB.3AH8 (23).

leads to low BMD through direct effects on osteoblasts. The mediators of such an effect, upstream or downstream of the mutant $G\alpha_{11}$, are unclear. Although short stature was reported in 2 families with ADH2 (12, 14), we did not detect a difference in weight or length between the mutant ADH2 mice and WT controls. Future experiments are necessary to define the full spectrum of effects of this gain-of-function mutation in $G\alpha_{11}$ on various GPCR-controlled signaling responses in different tissues.

In theory, gain-of-function $G\alpha_{11}$ mutants could either lead to enhanced downstream signaling independent of any upstream GPCR — as is seen with highly activating, oncogenic mutations — or increased signaling initiated by an activated GPCR. Our in vitro studies, measuring changes in Ca^{2+}_i as a measure of signaling via the IP_3/PLC/Ca^{2+}_i pathway detected an enhancement in CASR-mediated signaling in HEK-293–derived cells expressing the CASR and the GNA11^{R6OC} mutant. Babinsky et al. demonstrated similar enhancements in CASR signaling responsiveness with other $G\alpha_{11}$ gain-of-function variants — $G\alpha_{11}^{R181Q}$ and $G\alpha_{11}^{F341L}$ — found in ADH2 (25). The calcilytic NPS 2143, a NAM of CASR function, was shown to suppress the enhancing effects of the $G\alpha_{11}^{R181Q}$ and $G\alpha_{11}^{F341L}$ mutants on CASR signaling in cell-based assays (25). Likewise, we tested the same NAM on the GNA11^{R6OC} mutation and found that it could shift the calcium response curve to match that obtained with WT $G\alpha_{11}$. Moreover, NPS 2143 could partially rescue the calcium-homeostatic defects induced by these mutant $G\alpha_{11}$ proteins in mice. These findings suggest that further exploration of such CaSR-targeted inhibitor compounds might be a viable path toward new therapeutic strategies for ADH2. A potential benefit suggested by our current studies in the ADH2 mice (Figure 5) is that such a CASR-specific NAM could help reduce urinary calcium excretion by not only raising serum PTH via effects on the parathyroid glands, but also by having direct effects on CASR function in the distal tubule. The apparent lack of a

reduction in urinary fractional excretion of calcium by NPS 2143 in our WT mice is likely due, in part, to the limitations of our FEICa data, as only a single spot urine sample was collected and analyzed. The analysis of renal calcium handling in ADH2 is also complicated by the possibility that $G\alpha_{11}$ could couple to both the CASR and to the PTH receptor (PTH1R), which mediate opposing effects on renal calcium transport. Thus, more extensive studies on the renal handling of calcium and other mineral ions (e.g., sodium, phosphate, and magnesium), as well as on GFR and serum FGF23 levels, are needed to fully define the role of $G\alpha_{11}$ function in the kidney. The fact that the serum phosphate concentration increased in WT mice after calcilytic treatment — rather than decreased, as might be expected from the elevations in PTH — could be explained by excessive PTH-induced bone resorption, as the phosphate mobilized from the mineral matrix would exceed the short-term phosphate-excretion capacity of the kidney.

Overall, the response of the *GNA11*^{R60C} mice to treatment with a calcilytic is of considerable interest, as it suggests that the gain-of-function effect of the Arg60Cys mutation, which maps to helix-1 of the G protein, is at least partly dependent on coupling to the CASR. These findings are particularly interesting in the light of data from a recent Phase II clinical trial, which shows promise for calcilytics in patients with ADH1 (33). Our study supports the further exploration of these compounds for use in patients with ADH2.

Given that ADH2 arises from mutations in $G\alpha_{11}$, we explored the potential efficacy of a specific $G\alpha_{11/q}$ inhibitor, YM-254890, to correct the defects in calcium homeostasis in the ADH2 mice. YM-254890 is a cyclic depsipeptide that binds specifically to $G\alpha_{11}$ and $G\alpha_{q}$ and inhibits GDP release and hence activation of these two G proteins (23). It is a natural product that was first isolated from the bacterium *Chromobacterium sp.* as an inhibitor of ADP-induced platelet aggregation (22). Successful total synthesis has recently been reported (24). X-ray crystallography has shown that YM-254890 bound to $G\alpha_{q}$, which is very similar to $G\alpha_{11}$, interacts with switch 1 and hinders linker flexibility between the GTPase domain and the helical domain of the $G\alpha_{11/q}$ protein (Figure 8D). The decreased flexibility stabilizes the $G\alpha_{11/q}$ protein in the GDP-bound inactive state, therefore inhibiting $G\alpha_{11/q}$ activation (23). Our studies show for the first time to our knowledge that inhibition of $G\alpha_{11/q}$ in WT mice by this compound significantly increases blood calcium levels, presumably by increasing secretion of PTH. These observations also suggest that a low basal-state level of $G\alpha_{11}$ signaling in the parathyroid glands, induced by normal ambient blood calcium levels, acts to maintain a tonic suppression of PTH secretion. Treatment with the $G\alpha_{11/q}$ inhibitor releases this tonic suppression and increases PTH release. The published crystal structure of YM-254890 in complex with the related $G\alpha_{q}$ also revealed that the compound forms a key hydrogen bond with Arg60 of the G protein (23). The replacement of this Arg60 by cysteine, as in the mutant studied here, is therefore predicted to render the mutant G protein resistant to the inhibitory effect of YM-254890. The compound indeed showed lack of efficacy in homozygous mutant mice, confirming a critical role for the Arg60 residue in binding YM-254890 to $G\alpha_{11}$. We did, however, observe rescue effects of the compound in heterozygous mice as nonsignificant increases in PTH and calcium levels, which are likely due to the presence of the one WT $G\alpha_{11}$ allele. We conclude that the inhibitor requires the presence of at least one WT $G\alpha_{11}$ allele to function in the context of this particular ADH2 mutation.

The different effects of YM-254890 on WT vs. mutant $G\alpha_{11}$ in vivo are also consistent with our in vitro studies. We showed that YM-254890 failed to inhibit $Ca^{2+}{}_{i}$ signaling through the mutated $G\alpha_{11}{}^{R6OC}$, but it did inhibit signaling through the WT $G\alpha_{11}$. This supports the notion that the YM-254890 class of compounds should be further explored for therapeutic potential in the heterozygous disease ADH2, irrespective of the predicted sensitivity of the mutated allele to YM-254890.

In summary, we used CRISPR-Cas9 technology to create a mouse model of ADH2 harboring an activating mutation in *GNA11*. The *GNA11*^{R60C} mutant knockin mice mimic the human disease, with hypocalcemia and inappropriately low PTH levels demonstrating that this mutation is sufficient to cause ADH2. We also observed additional pathologies that have so far not been reported for ADH2 — namely increased skin pigmentation and low bone mineral density. Thus, this mouse model gives clues as to additional defects that might arise in patients with such an activating mutation in $G\alpha_{11}$.

We further show that the activity of the mutant G protein is at least partly dependent on coupling to the CASR and is, thus, quite distinct from the activity associated with the more widely known G protein activating mutations (e.g., $G\alpha_{S}{}^{R201H}$ found in McCune Albright Syndrome that directly affects the GTPase site, resulting in stronger, often oncogenic signaling effects that are not observed as inheritable

germline mutations). Treatment with the CASR-targeted calcilytic NPS 2143 effectively increased serum calcium and PTH levels in the mutant *GNA11*^{R60C} mice, suggesting its potential for treatment of ADH2. The specific $G\alpha_{11/q}$ inhibitor, YM-254890, was without efficacy in homozygous mice, reflecting the requirement for Arg60 in binding the drug; however, it increased serum calcium and PTH in heterozygous mice, and thus may be an alternative approach to therapy of ADH2 as well as other diseases involving alterations in $G\alpha_q$ or $G\alpha_{11}$ signaling.

Methods

Compounds. NPS 2143 hydrochloride (2-Chloro-6-[(2R)-3-[[1,1-dimethyl-2-(2-naphthalenyl)ethyl] amino]-2-hydroxypropoxy]-benzonitrile hydrochloride) was obtained from Sigma-Aldrich (catalog SML0362) and dissolved in a 20% aqueous solution of 2-hydroxypropyl-β-cyclodextrin (Sigma-Aldrich, catalog H107) prior to use in in vitro studies, as described (21, 25). YM-254890 was synthesized as previously described (24).

Cell culture and transfection. Functional studies were undertaken using a human *GNA11* construct (11), as the human and mouse $G\alpha_{11}$ proteins share an overall amino acid identity of 98% and are 100% identical in the region surrounding the mutated site. WT and mutant pBI-CMV2-*GNA11* expression constructs were generated as described (11). Site-directed mutagenesis was used to generate the mutant *GNA11* construct using the Quikchange Lightning Site-directed Mutagenesis kit (Agilent Technologies) and gene-specific primers (Sigma-Aldrich), as described (34). This bidirectional pBI-CMV2 vector allows for coexpression of $G\alpha_{11}$ and GFP at equivalent levels (11). Constructs were transiently transfected into HEK293 cells stably expressing CASR (HEK-CASR) using Lipofectamine 2000 (Invitrogen). Cells were maintained in DMEM-Glutamax media (Thermo Fisher Scientific) with 10% FBS (Gibco) and 400 μg/ml geneticin (Thermo Fisher Scientific) at 37°C, 5% CO_2. Successful transfection was confirmed by visualizing GFP fluorescence using an Eclipse E400 fluorescence microscope with a Y-FL Epifluorescence attachment and a triband 4,6-diamidino-2-phenylindole-FITC-Rhodamine filter, and images captured using a DXM1200C digital camera and NIS Elements software (Nikon) (11, 35). The expression of $G\alpha_{11}$ and CASR proteins was also determined by Western blot analysis using anti-$G\alpha_{11}$ (Santa Cruz Biotechnology Inc., sc-390382), anti-GFP (Santa Cruz Biotechnology Inc., sc-9996), anti-calnexin (Millipore, AB2301), or anti-CASR (AbCam, ab19347) antibodies. The Western blots were visualized using an Immuno-Star WesternC kit (Bio-Rad) on a Bio-Rad Chemidoc XRS+ system (11).

Ca^{2+}_i *measurements*. The Ca^{2+}_i responses of HEK293-CASR cells expressing WT or mutant $G\alpha_{11}$ proteins were assessed by a flow cytometry-based assay, as described (11, 35). In brief, HEK293-CASR cells were cultured in T75 flasks and transiently transfected 24 hours later with 16 μg DNA (11). Forty-eight hours following transfection, the cells were detached, resuspended in calcium-free (Ca^{2+}-free) and magnesium-free (Mg^{2+}-free) HBSS, and loaded with 1 μg/ml Indo-1-acetoxymethylester (Indo-1-AM, Molecular Probes) for 1 hour at 37°C. After removal of free dye, cells were resuspended in Ca^{2+}- and Mg^{2+}-free HBSS and maintained at 37°C. Transfected HEK-CASR cells were incubated with either a 20% aqueous solution of 2-hydoxypropyl-β-cyclodextrin (Sigma-Aldrich) (vehicle) or NAM NPS 2143 (Sigma-Aldrich) at concentrations of 10, 20, and 30 nM for 1 hour, as previously described (25). Transfected cells, in suspension, were stimulated by sequentially adding Ca^{2+} to the Ca^{2+}- and Mg^{2+}-free HBSS to increase the $[Ca^{2+}]_o$ in a stepwise manner from 0–15 mM, and then analyzed on a MoFlo modular flow cytometer (Beckman Coulter) by simultaneous measurements of GFP expression (at 525 nm), Ca^{2+}_i-bound Indo-1AM (at 410 nm), and free Indo-1AM (i.e., not bound to Ca^{2+}_i) (at 485 nm), using a JDSU Xcyte UV laser (Coherent Radiation) on each cell at each $[Ca^{2+}]_o$, as described (11, 35). The peak mean fluorescence ratio of the Ca^{2+}_i transient response after each individual stimulus was measured using Cytomation Summit software (Beckman Coulter) and expressed as a normalized response, as described (11, 35). Nonlinear regression of concentration-response curves was performed with GraphPad Prism using the normalized response at each $[Ca^{2+}]_o$ for each separate experiment for the determination of EC_{50} (i.e., $[Ca^{2+}]_o$ required for 50% of the maximal response) and Hill coefficient values (36). The maximal signaling response was measured as a fold-change of the peak transient Ca^{2+}_i response to the basal Ca^{2+}_i response measured at 0 mM $[Ca^{2+}]_o$ (36). The maximal signaling responses for mutant $G\alpha_{11}$ proteins were expressed as a percentage of the WT $G\alpha_{11}$ protein maximal signaling response. The mean EC_{50} and Hill coefficients obtained from 4 separate transfection experiments were used for statistical comparison by using the *F*-test, and alterations in maximal signaling responses assessed using the Mann-Whitney *U* test (36).

Ca^{2+} signaling and YM-254890. The effects of the $G\alpha_{11/q}$ specific inhibitor, YM-254890 (24, 37), on the PLC/IP_3/iCa^{2+} signaling capacities of $GNA11^{R60C}$ and $GNA11^{WT}$ were analyzed utilizing Fura-2–treated HEK-293–derived cells in which the genes encoding the endogenous $G\alpha_q$ and $G\alpha_{11}$ were knocked out (37). The cells were seeded in black 96-well plates and cotransfected using Lipofectamine 2000 (Thermo Fisher Scientific) with plasmids encoding either $GNA11^{R60C}$ or $GNA11^{WT}$, along with the PTHR1. The PTHR1 was chosen as a GPCR because it gives robust iCa^{2+} signaling responses in this assay format. The cells were analyzed 48 hours after transfection for PTH-induced Ca^{2+}_i signaling. The cells were, thus, pretreated for 45 minutes with media containing 5 μM Fura-2,AM (Invitrogen, f1221), with or without YM-254890 (30 μM to 10 nM); the cells were then rinsed and base-line ratiometric fluorescence (λ excitation 340 nm and 380 nm, λ emission, 515 nm) was measured using an Envision plate reader (PerkinElmer) for 14 seconds; the cells were then treated with hPTH(1-34) (100 nM), and measurements were continued for an additional 120 seconds. Dose-response curves for YM-254890 were generated by plotting the AUC for each PTH-induced response observed in the absence or presence of inhibitor.

CRISPR/Cas9 generation of $GNA11^{R60C}$ mice. Mice with the point mutation c.C178T (p.Arg60Cys) in *GNA11*, the gene encoding $G\alpha_{11}$, were generated by homology-directed repair using the CRISPR-Cas9 system. Single-guide RNAs (sgRNAs) targeting the region around the genomic sequence that codes for Arg60 were designed (http://crispr.mit.edu) and cloned into the pSpCas9n(BB)-2A-GFP plasmid (Addgene) (38). The efficacy of different sgRNA to create double-stranded DNA breaks was estimated by determining the frequency of mutations that were created in vitro in C3HT10½ cells using the TIDE algorithm (39). The sgRNA with the best efficiency in vitro, CCTCCGAGTAGCCGGCCCCG, was found to induce a DNA break in 67% of the sequences and was therefore selected for zygote injection. In vitro transcription of the guide RNA was performed as described by Yang et al. (40).

A single-strand DNA oligonucleotide template of 150 bp that contained the *GNA11* c.C178T mutation (p.Arg60Cys) and homology arms of 56 bp and 57 bp was synthesized. Nine other silent bp changes were incorporated to avoid guide recognition of the oligonucleotide template and to create a ScaI restriction site if the homology-directed repair was successful.

C57BL/6 mice zygotes (Charles River Laboratories) were injected with synthetic Cas9 RNA (System Biosciences Inc.), the purified sgRNA, and the oligonucleotide DNA template. The zygotes were implanted into 11 recipient dams.

Mice were housed in the Center for Comparative Medicine (CCM) at Massachusetts General Hospital (MGH) in conditions of 23°C with 40% humidity in a 12-hour light/dark cycle with wood bedding and igloo covers. Mice had free access to water and irradiated diet (when not fasting) consisting of 1.11% calcium, 0.48% phosphate, and 2.5 IU/g vitamin D. The mutant mice did not require a rescue diet.

Characterization of $GNA11^{R60C}$ mice. Founder mice were identified by isolating tail DNA and cloning the $GNA11^{R60}$ region into single clones, which were then sequenced. Founder mice were crossed with WT C57BL6 mice to generate the heterozygous F1 generation, which were crossed to yield the experimental animals. Male and female mice from 3 independent breeding lines were included in the experimental group. Genotyping for the presence of the Arg60Cys allele was performed by isolation of genomic DNA from mouse tail and PCR-amplification using primers 5'-CACAGTAGGTGGGCAGGACT-3' and 5'-GCCTCAAGGGCAGATACCTT-3'. The 325 bp PCR product was digested with ScaI to survey for the mutant allele.

At age 12–13 weeks, mice were sacrificed and their weight and length measured. In vivo measurements of whole-body (excluding the head) or hind limb BMD (g/cm^2) were obtained at time of sacrifice using peripheral DXA (PIXImus II, GE Lunar Corporation), as previously described (41).

μCT imaging was performed on the femurs of female and male mice. A high-resolution desktop micro-tomographic imaging system (μCT40, Scanco Medical AG) was used to assess bone mineral density, trabecular bone microarchitecture, and cortical bone morphology in the distal femoral metaphysis and mid-diaphysis. Scans were acquired using a 10 μm^3 isotropic voxel size at 70 kVP, 114 mAs, 200 ms integration time, and were subjected to Gaussian filtration and segmentation. Image acquisition and analysis protocols adhered to the Journal of Bone and Mineral Research (JBMR) guidelines (42). Trabecular bone was evaluated in a 1,500 μm (150 transverse slices) region beginning 200 μm above the peak of the distal growth plate and extending proximally. Trabecular bone was segmented from soft tissue using a threshold of 314 $mgHA/cm^3$, and the Scanco Evaluation program trabecular morphology script was used to measure bone volume fraction (BV/TV, %), trabecular thickness (Tb.Th, mm), Tb.N (1/mm), Tb.Sp (mm),

and trabecular BMD (Tb. BMD, mgHA/cm^3). Cortical bone was evaluated in a 500-μm long (50 transverse slices) at the femoral mid-diaphysis. Cortical bone was segmented using a threshold of 700 mgHA/cm^3 and then evaluated using the Scanco mid-shaft evaluation script to measure total cross-sectional area (Tt.Ar, mm^2), cortical bone area (Ct.Ar, mm^2), medullary area (Ma.Ar, mm^2), bone area fraction (Ct.Ar/Tt.Ar, %), cortical tissue mineral density (Ct.TMD, mgHA/cm^3), Ct.Th (mm), and cortical porosity (%), as well as maximum, minimum, and polar moments of inertia (Imax, Imin, and J, mm^4).

Treatment of mice with the calcilytic NPS 2143. Nine-week-old male and female mice were fasted for 6 hours before the start of the study and were provided water ad libitum. Mice were injected i.p. with a single bolus of either 28 mg/kg of the calcilytic NPS 2143 (Tocris Bioscience), diluted in 20% (2-hydroxypropyl)-β-cyclodextrin (Sigma-Aldrich) or an equal volume of 20% (2-hydroxypropyl)-β-cyclodextrin as the vehicle control. The dose of 30 mg/kg of the calcilytic NPS 2143 was previously shown to be effective in mouse models (21). Blood was taken from the superficial temporal vein at baseline, 4, and 24 hours after injection, and ionized calcium, PTH, and phosphate were measured as described (43). Ionized calcium values were corrected for pH. Spot urine was collected at baseline and, 4 hours after injection, was analyzed for calcium, phosphate, and creatinine (Stanbio Laboratory) (43).

Treatment of mice with YM-254890. Twelve-week-old male and female mice were fasted for 6 hours prior to the study and for the duration of the experiment, but water was provided ad libitum. Based on limited dose response studies (data not shown), mice were injected i.p. with either 0.15 mg/kg of the selective $G\alpha_{11/q}$ inhibitor YM-254890 (24), which was diluted in 0.27% DMSO, or an equal volume of 0.27% DMSO as the vehicle control. Blood was taken from the superficial temporal vein at baseline, 4, and 24 hours after injection, and ionized calcium, PTH, and phosphorous were measured as previously described (43). Spot urine was collected and analyzed for calcium, phosphate, and creatinine at baseline and 4 hours after injection (43). The FEICa was calculated by the equation: urine calcium/(urine creatinine × blood calcium) (44).

Statistics. Data were analyzed using Microsoft Excel 2011 and GraphPad Prism 6.0. The results are expressed as mean ± SD. When comparing 2 values, the Student's *t* test was performed (2-tailed, equal variances), and a $P < 0.05$ was considered statistically significant. When comparing more than 2 samples as in the baseline measurements, an ANOVA test was used with Tukey's multiple corrections test to compare the 3 groups.

Study Approval. This study was approved by the Institutional Animal Care and Use Committee (IACUC) of MGH.

Author Contributions

KLR and MM wrote the manuscript. MM conceived of and supervised the work. KLR and RB were responsible for designing and performing the mouse studies, with advice and supervision from MM and TG. AI generated and characterized the $G\alpha_{11/q}$ KO HEK cells. CMG performed in vitro studies with supervision from RVT. XFX, HBO, and KS synthesized the $G\alpha_{11/q}$ inhibitor YM-254890. KLR, RB, MM, TG, CMG, and RVT contributed to ideas in the construction of the manuscript.

Acknowledgments

This work was supported by the NIH grants R01-DK100584 (to MM) and T32DK007028 (supporting KR), the Center for Skeletal Research Imaging and Biomechanical Testing Core and the Center for Skeletal Research Core (NIH P30 AR066261), the UK Medical Research Council program grants (G9825289 and G1000467; to CG and RT), Wellcome Trust Investigator Award (to RT), NIH Research (NIHR) Oxford Biomedical Research Centre Programme (to RT), NIHR Senior Investigator Award (to RT), grants by JST, PRESTO (to AI), China State Key Laboratory of Oral Diseases Open Funding SKLOD2015OF01 (to RB), and a grant from the Lundbeck Foundation (to KS and HBO). We thank the Harvard genome modification facility for generating mice, Michael Armanini, Daniel Brooks, and Mary Bouxsein for skeletal imaging; Han Xie, Braden Corbin, and Monica Reyes for help with in vitro assays; Marc Wein for advice using CRISPR-Cas9; and Henry Kronenberg for comments on this manuscript.

Address correspondence to: Michael Mannstadt, Endocrine Unit, Massachusetts General Hospital, Thier 1123, 50 Blossom Street, Boston, Massachusetts 02114, USA. Phone: 617.726.3966; E-mail: mannstadt@mgh.harvard.edu.

1. Neves SR, Ram PT, Iyengar R. G protein pathways. *Science*. 2002;296(5573):1636–1639.
2. Flock T, et al. Universal allosteric mechanism for Gα activation by GPCRs. *Nature*. 2015;524(7564):173–179.
3. Spiegel AM, Weinstein LS. Inherited diseases involving g proteins and g protein-coupled receptors. *Annu Rev Med*. 2004;55:27–39.
4. Van Raamsdonk CD, et al. Frequent somatic mutations of GNAQ in uveal melanoma and blue naevi. *Nature*. 2009;457(7229):599–602.
5. Van Raamsdonk CD, et al. Mutations in GNA11 in uveal melanoma. *N Engl J Med*. 2010;363(23):2191–2199.
6. Shirley MD, et al. Sturge-Weber syndrome and port-wine stains caused by somatic mutation in GNAQ. *N Engl J Med*. 2013;368(21):1971–1979.
7. Ayturk UM, et al. Somatic Activating Mutations in GNAQ and GNA11 Are Associated with Congenital Hemangioma. *Am J Hum Genet*. 2016;98(6):1271.
8. Happle R. The McCune-Albright syndrome: a lethal gene surviving by mosaicism. *Clin Genet*. 1986;29(4):321–324.
9. Iiri T, Herzmark P, Nakamoto JM, van Dop C, Bourne HR. Rapid GDP release from Gs alpha in patients with gain and loss of endocrine function. *Nature*. 1994;371(6493):164–168.
10. Mannstadt M, et al. Germline mutations affecting Gα11 in hypoparathyroidism. *N Engl J Med*. 2013;368(26):2532–2534.
11. Nesbit MA, et al. Mutations affecting G-protein subunit α11 in hypercalcemia and hypocalcemia. *N Engl J Med*. 2013;368(26):2476–2486.
12. Li D, et al. Autosomal dominant hypoparathyroidism caused by germline mutation in GNA11: phenotypic and molecular characterization. *J Clin Endocrinol Metab*. 2014;99(9):E1774–E1783.
13. Piret SE, et al. Identification of a G-Protein Subunit-α11 Gain-of-Function Mutation, Val340Met, in a Family With Autosomal Dominant Hypocalcemia Type 2 (ADH2). *J Bone Miner Res*. 2016;31(6):1207–1214.
14. Tenhola S, Voutilainen R, Reyes M, Toiviainen-Salo S, Jüppner H, Mäkitie O. Impaired growth and intracranial calcifications in autosomal dominant hypocalcemia caused by a GNA11 mutation. *Eur J Endocrinol*. 2016;175(3):211–218.
15. Hofer AM, Brown EM. Extracellular calcium sensing and signalling. *Nat Rev Mol Cell Biol*. 2003;4(7):530–538.
16. Conigrave AD, Ward DT. Calcium-sensing receptor (CaSR): pharmacological properties and signaling pathways. *Best Pract Res Clin Endocrinol Metab*. 2013;27(3):315–331.
17. Pollak MR, et al. Autosomal dominant hypocalcaemia caused by a Ca(2+)-sensing receptor gene mutation. *Nat Genet*. 1994;8(3):303–307.
18. Kantham L, et al. The calcium-sensing receptor (CaSR) defends against hypercalcemia independently of its regulation of parathyroid hormone secretion. *Am J Physiol Endocrinol Metab*. 2009;297(4):E915–E923.
19. Shoback D. Clinical practice. Hypoparathyroidism. *N Engl J Med*. 2008;359(4):391–403.
20. Nemeth EF, et al. Calcilytic compounds: potent and selective Ca2+ receptor antagonists that stimulate secretion of parathyroid hormone. *J Pharmacol Exp Ther*. 2001;299(1):323–331.
21. Hannan FM, et al. The Calcilytic Agent NPS 2143 Rectifies Hypocalcemia in a Mouse Model With an Activating Calcium-Sensing Receptor (CaSR) Mutation: Relevance to Autosomal Dominant Hypocalcemia Type 1 (ADH1). *Endocrinology*. 2015;156(9):3114–3121.
22. Takasaki J, et al. A novel Galphaq/11-selective inhibitor. *J Biol Chem*. 2004;279(46):47438–47445.
23. Nishimura A, et al. Structural basis for the specific inhibition of heterotrimeric Gq protein by a small molecule. *Proc Natl Acad Sci US A*. 2010;107(31):13666–13671.
24. Xiong XF, et al. Total synthesis and structure-activity relationship studies of a series of selective G protein inhibitors. *Nat Chem*. 2016;8(11):1035–1041.
25. Babinsky VN, et al. Allosteric Modulation of the Calcium-sensing Receptor Rectifies Signaling Abnormalities Associated with G-protein α-11 Mutations Causing Hypercalcemic and Hypocalcemic Disorders. *J Biol Chem*. 2016;291(20):10876–10885.
26. Saggio I, et al. Constitutive expression of Gsα(R201C) in mice produces a heritable, direct replica of human fibrous dysplasia bone pathology and demonstrates its natural history. *J Bone Miner Res*. 2014;29(11):2357–2368.
27. Pearce SH, et al. A familial syndrome of hypocalcemia with hypercalciuria due to mutations in the calcium-sensing receptor. *N Engl J Med*. 1996;335(15):1115–1122.
28. Van Raamsdonk CD, Fitch KR, Fuchs H, de Angelis MH, Barsh GS. Effects of G-protein mutations on skin color. *Nat Genet*. 2004;36(9):961–968.
29. Rubin MR, et al. Dynamic and structural properties of the skeleton in hypoparathyroidism. *J Bone Miner Res*. 2008;23(12):2018–2024.
30. Shoback DM, et al. Presentation of Hypoparathyroidism: Etiologies and Clinical Features. *J Clin Endocrinol Metab*. 2016;101(6):2300–2312.
31. Dong B, et al. Calcilytic Ameliorates Abnormalities of Mutant Calcium-Sensing Receptor (CaSR) Knock-In Mice Mimicking Autosomal Dominant Hypocalcemia (ADH). *J Bone Miner Res*. 2015;30(11):1980–1993.
32. Ogata N, Kawaguchi H, Chung UI, Roth SI, Segre GV. Continuous activation of G alpha q in osteoblasts results in osteopenia through impaired osteoblast differentiation. *J Biol Chem*. 2007;282(49):35757–35764.
33. Ramnitz M, et al. 2015. Treatment of Autosomal Dominant Hypocalcemia with the Calcilytic NPSP795 [ASBMR abstract S472]. *J Bone Miner Res.* 2015;30:(Suppl 1).
34. Newey PJ, et al. Mutant prolactin receptor and familial hyperprolactinemia. *N Engl J Med*. 2013;369(21):2012–2020.
35. Nesbit MA, et al. Mutations in AP2S1 cause familial hypocalciuric hypercalcemia type 3. *Nat Genet*. 2013;45(1):93–97.
36. Gorvin CM, et al. A G-protein Subunit-α11 Loss-of-Function Mutation, Thr54Met, Causes Familial Hypocalciuric Hypercalcemia Type 2 (FHH2). *J Bone Miner Res*. 2016;31(6):1200–1206.
37. Schrage R, et al. The experimental power of FR900359 to study Gq-regulated biological processes. *Nat Commun*. 2015;6:10156.
38. Ran FA, Hsu PD, Wright J, Agarwala V, Scott DA, Zhang F. Genome engineering using the CRISPR-Cas9 system. *Nat Protoc*. 2013;8(11):2281–2308.
39. Brinkman EK, Chen T, Amendola M, van Steensel B. Easy quantitative assessment of genome editing by sequence trace decomposition. *Nucleic Acids Res*. 2014;42(22):e168.
40. Yang H, Wang H, Jaenisch R. Generating genetically modified mice using CRISPR/Cas-mediated genome engineering. *Nat*

Protoc. 2014;9(8):1956–1968.

41. Bouxsein ML, Seeman E. Quantifying the material and structural determinants of bone strength. *Best Pract Res Clin Rheumatol*. 2009;23(6):741–753.
42. Bouxsein ML, Boyd SK, Christiansen BA, Guldberg RE, Jepsen KJ, Müller R. Guidelines for assessment of bone microstructure in rodents using micro-computed tomography. *J Bone Miner Res*. 2010;25(7):1468–1486.
43. Bi R, et al. Diphtheria Toxin- and GFP-Based Mouse Models of Acquired Hypoparathyroidism and Treatment With a Long-Acting Parathyroid Hormone Analog. *J Bone Miner Res*. 2016;31(5):975–984.
44. Guo J, Khatri A, Maeda A, Potts JT, Jüppner H, Gardella TJ. Prolonged Pharmacokinetic and Pharmacodynamic Actions of a Pegylated Parathyroid Hormone (1-34) Peptide Fragment. *J Bone Miner Res*. 2017;32(1):86–98.